Arabian Journal for Science and Engineering
https://doi.org/10.1007/s13369-026-11154-9

RESEARCH ARTICLE-CIVIL ENGINEERING

Blasting Resistance of Sandwich Bunkers with Carbon Fiber Reinforced Polymer Skins and Polymer Concrete Core

Mahmudul Hasan[1] · **Ahmad B. H. Kueh**[1,2]

Received: 22 April 2025 / Accepted: 3 February 2026

Abstract

The blast resistance of sandwich polymer concrete core bunkers (SPCB) with CFRP skins versus sandwich concrete core bunkers (SCB) is examined using ABAQUS/Explicit incorporating CONWEP feature. Investigation is conducted for varying TNT masses (1–25 kg), standoff distances (0.1–1 m), and core thicknesses (200–500 mm). Findings reveal that ABAQUS/Explicit with CONWEP accurately describes blasting behavior against existing laboratory and numerical results alongside the observation that increasing deflection, stress, and perforation damage correlate with higher blast masses, reduced distances, and thinner cores. SPCBs outperform SCBs, with the 500 mm thick SCB sustaining 34.8% more damage from a 25 kg TNT explosion at 1 m. SPCBs at 1 m demonstrate 80–99% greater performance while exhibiting superior blast resilience and seldom perforate compared to SCBs. From all results, robust regression equations for accurate predictions of principal and von Mises stresses based on core thickness, TNT mass, and standoff distance are established for future design convenience.

Keywords Blast resistance · Sandwich polymer concrete bunker · CFRP skin · Perforation · TNT mass · Stand-off distance

1 Introduction

In recent years, the world has experienced increased terrorist and military attacks involving explosions and impacts. This has raised public concerns about the potential collapse of major infrastructures, property damages, and worst human injuries and casualties [1]. In 2005, the US Department of State reported over 11,000 terrorist attacks globally, resulting in the deaths of more than 14,600 individuals [2]. These figures emphasize the significant threat posed by terrorism worldwide. In 2018 alone, an alarming 55.2% of terror attacks were specifically targeted at buildings and infrastructures globally [3, 4]. The collapse of entire structures, exemplified by the Alfred P. Murrah Building in Oklahoma City, often leads to a significant loss of life. In this tragic event, approximately 87% of individuals in the collapsed section perished, with 153 out of 175 fatalities, compared to only 5% in the un-collapsed area, with 10 out of 186 casualties [5]. This finding serves as a stark reminder of the pressing need to safeguard critical structures against potential acts of aggression. As societies strive to uphold their security and resilience, understanding the factors contributing to structural integrity and devising effective preventive measures have become paramount in the global effort to mitigate such catastrophic outcomes.

To date, numerous studies have focused on exploring and refining methods and techniques for both explosion-proofing and fire-proofing, aiming to enhance structural resilience and safety [6–8]. Studies are available also on assessing the vulnerability and damage of various concrete elements, including pre-stressed concrete (PSC) and pre-stressed concrete containment vessels (PCCVs), under extreme loading conditions [9–14]. Current developments in polymer concrete recognize its superior blast resistance compared to traditional concrete and other building materials [15–17]. Retrofitting existing concrete structures is one way to bolster their resilience against impact and blast loads during their service life [2, 5, 16, 18]. Research recommends that reinforcing concrete with fibers could boost buildings' ability to withstand airplane collisions, potentially minimizing

✉ Ahmad B. H. Kueh
kbhahmad@unimas.my

1 Department of Civil Engineering, Faculty of Engineering, Universiti Malaysia Sarawak, 94300 Kota Samarahan , Sarawak , Malaysia

2 UNIMAS Water Centre (UWC), Faculty of Engineering, Universiti Malaysia Sarawak, 94300 Kota Samarahan , Sarawak , Malaysia

Published online: 30 March 2026

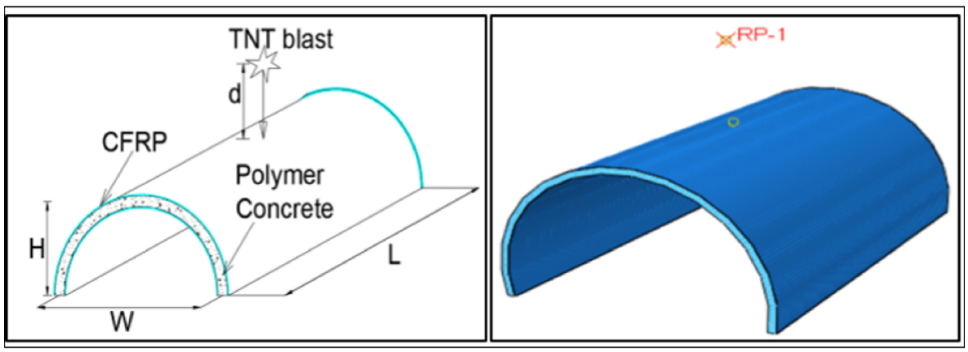

Fig. 1 **a** Sandwich bunker diagram and **b** proposed ABAQUS model

damage and enhancing structural integrity [4, 16]. Therefore, fiber-reinforced polymers (FRPs) such as CFRP, polyuria (PU), and glass fiber-reinforced polymer (GFRP) have gained significant prominence as potential blast-resisting materials [19, 20]. These materials are favored for their ability to increase concrete structure stiffness, enhance ductility, and improve energy absorption, rendering them valuable options for blast retrofitting endeavors [21, 22]. The application of FRP composite materials to retrofit concrete structural elements has proven highly effective in substantially enhancing their strength and stiffness [23–28]. Jahami et al. [29] conducted an experiment investigating the blasting response of RC beams retrofitted with CFRP using the ABAQUS/Explicit finite element software, incorporating CONWEP (Conventional Weapons Effects Program) and the concrete damage plasticity model, both approaches of which attain good correlation.

Having realized these material prospects, it is, nonetheless, worthwhile to emphasize that limited researchers have focused on the dynamic analysis of military bunkers exposed to blast loads over time [30, 31]. The primary purpose of bunkers is to redirect assaulting bombs away from people and vital areas to prevent bodily harm and property damage. Reflected overpressure, defined as pressure above atmospheric pressure caused by a shockwave, plays a critical role in minimizing damage to blasted structures. Given the observed benefits of CFRP in enhancing resistance and the scant research on bunker structures' blasting responses, the current study employs ABAQUS software to examine cylindrical bunkers with reinforced concrete cores sandwiched between CFRP skins under blast loading. The bunker design draws inspiration from the Hardened Aircraft shelter, as shown in Fig. 1 [32], using three layers of CFRP on the top and bottom to encase a concrete core [33–36].

The novelty of this study lies in its comprehensive numerical investigation of sandwich polymer concrete core bunkers (SPCBs) with CFRP skins, benchmarked against conventional sandwich concrete bunkers (SCBs) under diverse blast loading scenarios. While previous research has addressed FRP-reinforced structures and general blast resistance, this work uniquely focuses on the responses of cylindrical SPCBs, systematically assessed across a wide spectrum of TNT charges (1–25 kg), standoff distances (0.1–1 m), and core thicknesses (200–500 mm) using ABAQUS/Explicit with the CONWEP feature. The study not only demonstrates the superior blast resilience of SPCBs through comparative analysis but also introduces regression-based predictive models for stress responses.

Therefore, the study aims to investigate the effects of varying core thicknesses, TNT blast masses, and standoff distances on the structural responses of semi-circular cross-sectioned cylindrical sandwich polymer concrete bunkers with CFRP skins under blast loading. Additionally, the blast responses are compared with bunkers with a plain concrete core. Based on the simulation outcomes, the study further develops statistical predictive equations to forecast blast responses, providing valuable guidance for the design of future blast-resistant bunker structures.

2 Modeling Specifics

2.1 Simulation Set-Up

Figure 1b illustrates the sandwich bunker is modeled using the ABAQUS/Explicit 6.14 software as a semi-circular cross-section with 3.5 m (height, H) × 6.5 m (width, W) × 10 m (length, L) dimensions. The polymer concrete core is graded with a compressive strength of $f_c = 58.21$ MPa [37]. At both the top and bottom regions, 12 mm reinforcing rebar meshes are located with 150 mm spacing (T12@150 mm). Also, 12 mm rebars are used for shear reinforcement [38]. Core thicknesses of 200, 250, 300, and 500 mm are considered [39], with 3 mm-thick [0/ ± 30] CFRP skins sandwiching the top and bottom of the concrete core. Table 1 presents the key parameters used in this study. The characteristics of the

Table 1 Summary of key parameters

Parameter	Value
Bunker dimension (m)	3.5 (height) × 6.5 (width) × 10 (length)
Core thickness (mm)	200, 250, 300, 500
Polymer concrete compressive strength, f_c (MPa)	58.21
Polymer concrete density (kg/m^3)	2001
Polymer concrete Young's modulus (GPa)	36.09
Polymer concrete Poisson's ratio	0.20
Reinforcement (main &shear)	12 mm bars @ 150 mm spacing (T12@150)
TNT mass (kg)	1, 5, 10, 25
Standoff distance (m)	0.1, 0.25, 0.5, 1

Table 2 Properties of CFRP [37, 41]

Property	Value
Density, ρ (kg/m^3)	1,600
Longitudinal stiffness, E_1 (MPa)	138,580
Transverse stiffness, E_2 (MPa)	10,070
Poisson's ratio	0.2
In-plane shear stiffness, G_{12} (MPa)	5,129
Out-of-plane shear stiffness, G_{13} (MPa)	2,950
Out-of-plane shear stiffness, G_{23} (MPa)	5,129
Longitudinal tensile peak stress, X_t (MPa)	1,034.21
Longitudinal compressive peak stress, X_c (MPa)	689.48
Transverse tensile peak stress, Y_t (MPa)	41.37
Transverse compressive peak stress, Y_c (MPa)	117.21
Longitudinal shear peak stress, S_t (MPa)	68.95
Transverse shear peak stress, S_c (MPa)	68.95
CFRP skin thickness (mm)	3
CFRP maximum strain	0.015

CFRP material adopted to model the skins for the bunkers are listed in Table 2. It is assumed as an elastic material until it reaches failure.

The selection of core thicknesses, 200 mm, 250 mm, 300 mm, and 500 mm, is based on practical design standards for protective military and infrastructure elements subjected to blast loading, as well as previous studies that investigated structural performance under extreme conditions [39]. These thicknesses represent a realistic range found in existing reinforced concrete bunkers and shelters, balancing structural capacity, material usage, and space constraints. This thickness variation allows for a comprehensive analysis of how increasing thickness influences energy absorption, stress distribution, and perforation resistance under different blast intensities.

The material specifications for the polymer concrete include a density of 2001 kg/m^3, Young's modulus of 36.09 GPa, and Poisson's ratio of 0.2 [37]. The concrete damage plasticity (CDP) model has been chosen as the material description for the core due to its exceptional capability to accurately represent the comprehensive inelastic tension and compression damage characteristics of concrete. It adopts the stress–strain relationship proposed by Tao and Chen [40] to describe concrete under uniaxial compression. The experimentally measured compressive stress is defined by

$$\sigma_c = \frac{E_o \varepsilon_c}{1 + \left(\frac{E_o \varepsilon_p}{\sigma_p} - 2\right)\left(\frac{\varepsilon_c}{\varepsilon_p}\right) + \left(\frac{\varepsilon_c}{\varepsilon_p}\right)^2} \tag{1}$$

where ε_c denotes the experimental strain. Also, σ_p represents the experimental maximum stress and ε_p is the experimental maximum strain. The elastic modulus of concrete, denoted as E_o, is calculated using the formula $E_o = 4730\sqrt{f_c}$ [40, 42].

Converting stress and strain (Eqs. (2) and (3)) to their true counterparts ensures compatibility and accuracy within the ABAQUS simulation. This enables a precise representation of the material's mechanical behavior, accounting for changes in cross-sectional area and providing reliable analysis under different loading conditions where σ_{true} is the true stress and ε_{true} is the true strain.

$$\sigma_{true} = \sigma_c(1 + \varepsilon_c) \tag{2}$$

$$\varepsilon_{true} = ln(1 + \varepsilon_c) \tag{3}$$

The inelastic strain, $\varepsilon_{inelastic}$, is defined as

$$\varepsilon_{inelastic} = \varepsilon_{true} - \frac{\sigma_{true}}{E_0} \tag{4}$$

The compressive damage parameter, d_c, denotes the proportion of inelastic strain to total strain, signifying material damage under compression, while σ_p signifies the experimentally determined maximum stress.

$$d_c = 1 - \frac{\sigma_{true}}{\sigma_p} \tag{5}$$

The CDP model is commonly employed when concrete experiences stress or strain levels that surpass its ability to deform elastically. Under such conditions, concrete undergoes significant inelastic behavior, leading to cracking, crushing, and strain-softening [43, 44]. The CDP model is characterized by the post-peak stress–strain curve portion,

which is obtained from measured values and described using Eqs.(2–4).

Under uniaxial tension, the issue revolves around tensile cracking, with f_t representing the concrete uniaxial tensile strength. The parameter f_t represents the maximum tensile stress that the concrete can withstand before fracturing under tension.

$$f_t = 1.4\left(\frac{f_c - 8}{10}\right)^{\frac{2}{3}} \text{MPa} \tag{6}$$

The tensile damage parameter, d_t, is the ratio of cracking strain to total strain, reflecting material damage under tensile loading.

$$d_t = 1 - \frac{\sigma_{true}}{\sigma_p} \tag{7}$$

This study details the simulation method used to model the interface between CFRP and concrete in a sandwich bunker system, highlighting the material models, contact algorithms, and interaction mechanisms involved. The CFRP skins are modeled as linearly elastic up to a failure strain of 0.015, following data from Shakil and Hassan and Hasan and Kueh [37, 45], while the concrete core utilizes the Concrete Damaged Plasticity (CDP) model to capture nonlinear behavior under dynamic loading. Steel reinforcements are attached within the concrete using the embedded region technique, ensuring compatible deformation without the need for additional contact definitions. The CFRP concrete interface is defined using a surface-to-surface tie constraint, assuming perfect adhesion to simulate effective load transfer during blast events. This tied interaction plays a crucial role in distributing blast-induced stresses from the CFRP to the concrete core, directly influencing the structural response and enhancing the accuracy of predictive models.

CONWEP (Conventional Weapons Effects Program) is a widely utilized blast simulation model designed to replicate the pressure waves generated by explosive devices. In ABAQUS, CONWEP generates a blast pressure–time history based on input data, which can be applied to a structural model to simulate the effects of an explosion. Subsequently, the dynamic response of the structure is analyzed. The study considers TNT explosives placed at different standoff distances of 0.1, 0.25, 0.5, and 1 m from above the center of the bunker (see Fig. 1b), with TNT charges varied at 1, 5, 10, and 25 kg. Appropriate boundary conditions are applied, with two long sides of the bunker fixed (no translations and rotations in all directions), while the front and rear regions of the model are assumed free. Through this comprehensive analysis, the research aims to gain insights into how different core thicknesses, TNT masses, and standoff distances influence the blast performance of the sandwich concrete bunker.

Table 3 Summary of the converged node and element numbers of bunkers with different core thicknesses

Model code	Number of nodes	Number of elements
SPCB-200	195,846	176,410
SPCB-250	218,551	196,280
SPCB-300	246,131	220,800
SPCB-500	275,150	246,560

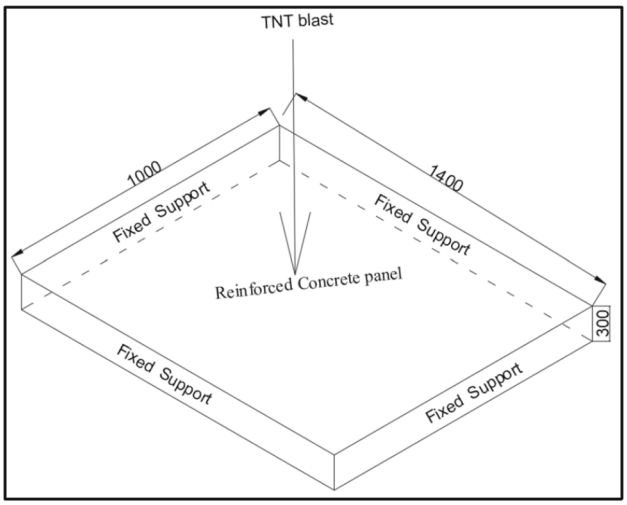

Fig. 2 Blasting on reinforced concrete panel (units:mm)

The converged node and element numbers for the sandwich polymer concrete bunker (SPCB) models with various core thicknesses are listed in Table 3. Here, the model code "SPCB-500-1" refers to a sandwich polymer concrete bunker with a core thickness of 500 mm in the presence of 1 kg equivalent TNT mass as the applied blasting load. In comparison, bunker models with conventional concrete with the codename SCB will also be constructed.

2.2 Verification

For verification, a reinforced concrete (RC) panel subjected to blasting investigated by Shishegaran et al.[4] depicted in Fig. 2 is replicated and compared. The RC panel is measured at 1400 × 1000 × 300 mm and reinforced with D13 steel rebar spaced at 100 mm intervals in two perpendicular directions. The concrete's material properties include a density of 2350 kg/m^3, Young's modulus of 30 GPa, compressive strength of 40 MPa, and Poisson's ratio of 0.15. The panel is fixed-supported on all its exterior vertical surfaces and is subjected to a 25 kg TNT blast load for 50 ms.

Figure 3 illustrates that the present modeling methodology closely captures the deflection-time curve of the plate in terms of both experimental and modeling techniques [3, 4].

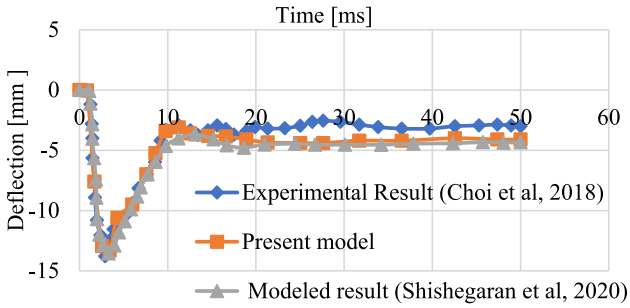

Fig. 3 Verification of blasting modeling technique of deflection-time curves

Overall, the relatively low difference percentage between the model and the actual data affirms the accuracy of the model. The present model is in 95–99% agreement with both the experimental and modeled results, thus verifying the simulation methodology with high accuracy and reliability.

An additional validation for the present computational methodology is conducted by replicating the computational study of Mohammadzadeh et al. [46]. In this verification, a steel plate with a Young's modulus of 200 GPa, density of 7850 kg/m^3, and Poisson's ratio of 0.3 is subjected to a 1 kg TNT blast load for 1.8 ms. The homogeneous, isotropic, and linear elastic plate, measured 1000 mm × 2000 mm × 10 mm, is pinned along exterior edges. The close agreement between the current simulation and the reference study, with a maximum normalized central deflection ($d_{\max}/h = 0.5$) deviation of only 1%, further confirms the reliability and accuracy of the blasting modeling approach used in this study.

3 Result and Discussion

3.1 Blasting Displacement of SCB Versus SPCB

Figure 4 displays the maximum vertical displacement experienced by different sandwich concrete bunker (SCB and SPCB) models when exposed to TNT explosions at varying distances.

The SCB-200-1 bunker is exposed to a TNT mass at 0.1 m with a maximum displacement measuring 30.6 mm. When the TNT source is located 1 m from the bunker's top, the maximum displacement significantly reduces to 0.21 mm. Similar trends are observed for the SCB-250-1 bunker. At 0.1 m blast distance, the maximum displacement is 28.7 mm, decreasing to 0.16 mm at 1 m, with zero displacements recorded at 2 m and 2.5 m distances. The response of the bunkers to the blast does not appear to be significantly affected by the variation in thickness. However, the SCB-500-1 bunkers exhibit a noticeable reduction in maximum displacement compared to SCB-200-1 and SCB-250-1. At 0.1 m, the largest displacement is only 22.0 mm, while at 1 m, it is a mere 0.158 mm, with no displacements at 2 m and 2.5 m.

The thicker bunker's ability to better withstand the explosion is demonstrated. As the TNT mass exposure increases, the displacements generally grow. For instance, in the case of the SCB-200-10 bunker, subjected to a blast distance of 0.1 m, the bunker cannot withstand the high TNT mass at proximity. At a 0.25 m standoff distance, the SCB models experience severe structural failure when subjected to greater TNT masses of 10 kg and 25 kg, resulting in computational termination. At a 1 m distance, the maximum displacement is 8.66 mm. Similar trends are observed for SCB-250-10, SCB-500-10, SCB-250-25, and SCB-500-25 bunkers when exposed to 10 kg and 25 kg TNT masses. When the TNT source is positioned 0.1 m from the bunker, the bunkers cannot withstand the high TNT mass nearby. For instance, the displacement for the SCB-250-10 bunker at a blast distance of 1 m from the top of the bunker is 7.29 mm. Meanwhile, for the SCB-500-10 bunker under the same conditions, the maximum displacement is 5.44 mm.

Lastly, for the SCB-200-25 bunker, at a 1 m blast distance from the top of the bunker, the maximum displacement is 22.0 mm. Similarly, for the SCB-250-25 bunker, the maximum displacement is 20.01 mm under the same conditions. For the SCB-500-25 bunker, the maximum displacement is 11.8 mm.

At a proximity of 0.1 m, when subjected to a 1 kg TNT mass, SPCB-200-1, SPCB-250-1, SPCB-300-1, and SPCB-500-1 exhibit maximum displacements of 6.13 mm, 5.14 mm, 3.74 mm, and 0.16 mm, respectively. Nevertheless, when the TNT mass is increased to 5 kg at the same distance, the displacements intensify, with the SPCB-200-5, SPCB-250-5, SPCB-300-5, and SPCB-500-5 models recording displacements of 36 mm, 24.9 mm, 18.2 mm, and 6.52 mm, respectively. It is worth noting that at a distance of 0.1 m and facing TNT masses of 10 kg and 25 kg, none of the SPCB models, regardless of their thickness (200 mm, 250 mm, 300 mm, and 500 mm) can effectively withstand the tremendous explosive forces.

At a slightly greater distance of 0.25 m, the SPCB models exposed to a 1 kg TNT mass display displacements of 2.24 mm, 1.9 mm, 1.49 mm, and 0.56 mm, respectively. Under a 5 kg TNT mass at the same distance, the displacements increase to 12.1 mm, 10.7 mm, 7.86 mm, and 3.72 mm, respectively. However, at a distance of 0.25 m and facing TNT masses of 10 kg and 25 kg, the SPCB models face challenges. The peak displacements for SPCB-200-10, SPCB-250-10, SPCB-300-10, and SPCB-500-10 are measured at 54.6 mm, 37.3 mm, 27.55 mm, and 11.2 mm, respectively. When a 25 kg TNT weight is applied, the

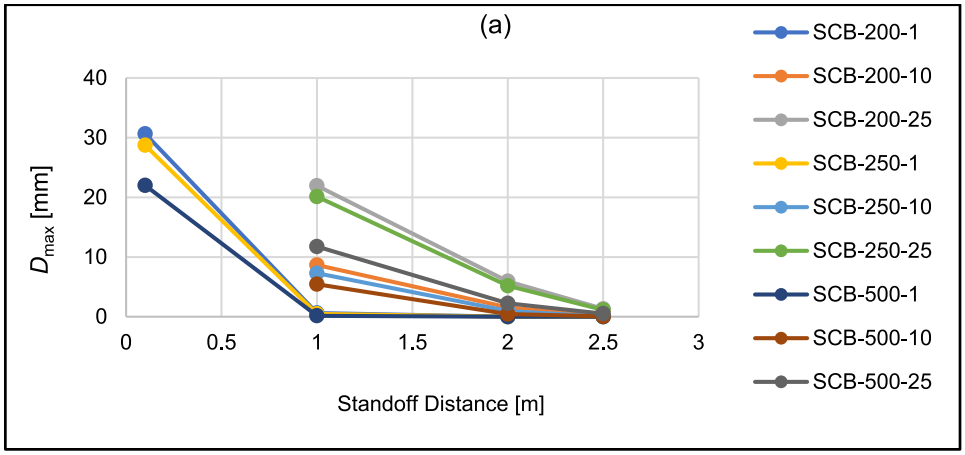

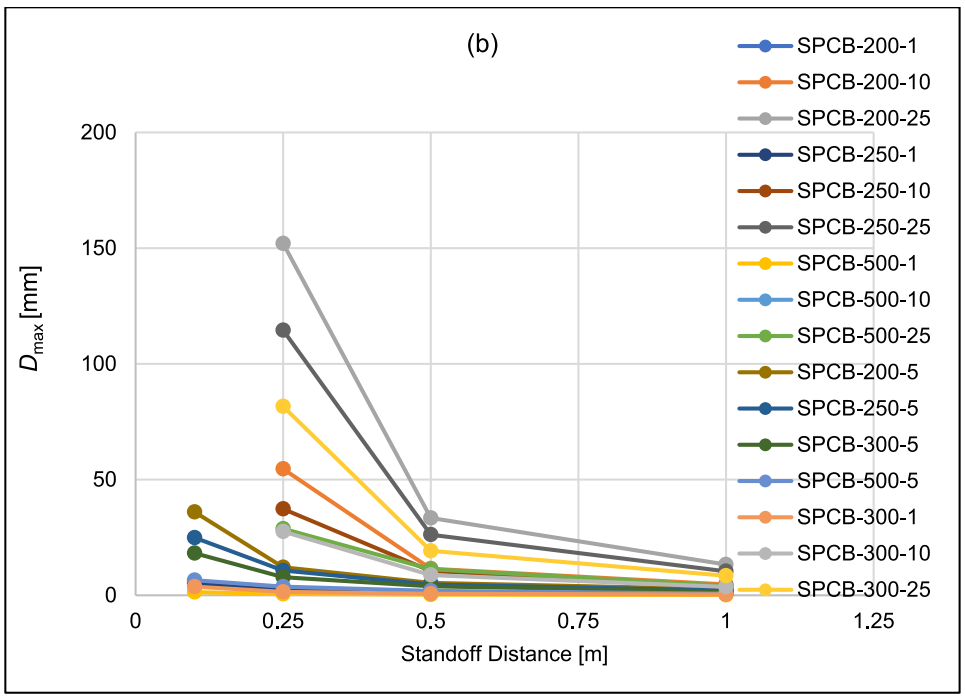

Fig. 4 Maximum vertical displacement of **a** SCB and **b** SPCB models

results significantly increase, with SPCB-200-25, SPCB-250-25, SPCB-300-25, and SPCB-500-25 showing displacements of 152 mm, 114.5 mm, 81.59 mm, and 28.76 mm, respectively.

At 0.5 m, the SPCB models, subjected to a 1 kg TNT mass, exhibit relatively modest displacements ranging from 0.28 to 1.1 mm. With a 5 kg TNT mass, the displacements increase to 1.95 mm, 3.9 mm, 4.69 mm, and 5.39 mm for the respective models.

When subjected to a 1 kg TNT mass at a standoff distance of 1 m, SPCB-200-1, SPCB-250-1, SPCB-300-1, and SPCB-500-1 experience peak displacements of 0.62 mm, 0.49 mm, 0.37 mm, and 0.16 mm, respectively. With a 5 kg TNT mass, the maximum displacements increase to 2.63 mm, 2.10 mm, 1.65 mm, and 0.72 mm. When exposed to a substantial 10 kg TNT mass, the greatest displacements further rise, measuring 4.7 mm, 3.91 mm, 3.63 mm, and 2.04 mm, respectively. Under the influence of a significant 25 kg TNT mass, the SPCB models exhibit notable peak displacements, with SPCB-200-25, SPCB-250-25, SPCB-300-25, and SPCB-500-25 registering 13.3 mm, 10.36 mm, 8.45 mm, and 4.16 mm, respectively. In comparison, SPCB-200-1, SPCB-250-1, and SPCB-500-1 are 80%, 82%, and 99% more potent than SCB-200-1, SCB-250-1, and SCB-500-1, respectively, based on 1 m standoff distance.

3.2 Principal Stress Distribution of SCB Versus SPCB

Figure 5 plots the principal stress distribution of bunkers subjected to a 1 kg TNT explosion at 1 m. SCB-200-1

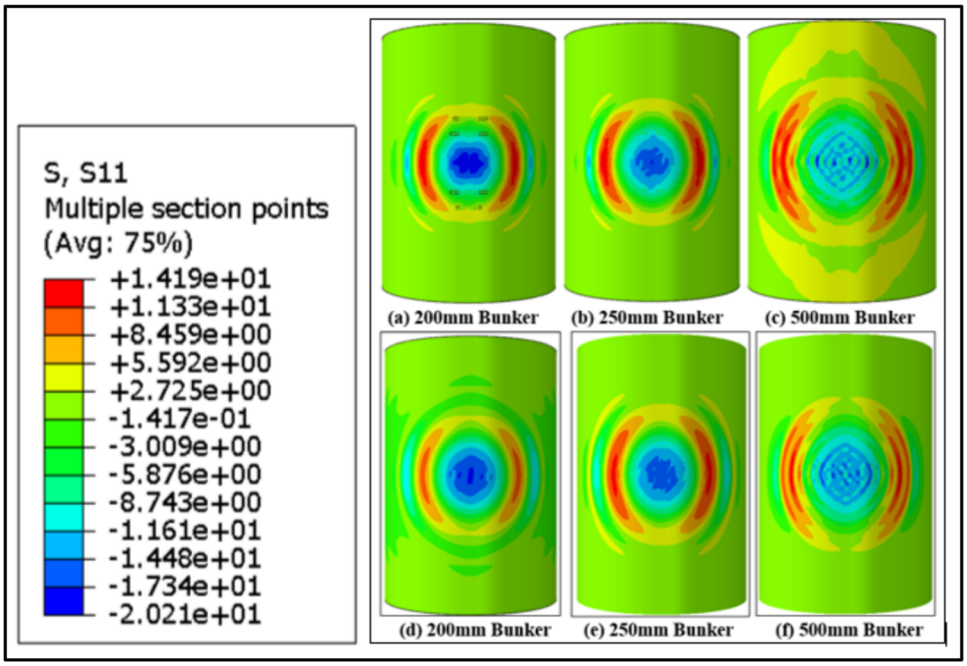

Fig. 5 Principal stress distribution plots at a distance of 1 m of **a** SCB-200-1, **b** SCB-250-1, **c** SCB-500-1, and **d** SPCB-200-1, **e** SPCB-250-1, **f**SPCB-500-1

exhibits elevated stress levels compared to bunkers of other thicknesses, such that it experiences element deletions, causing perforation and reducing its capacity to fully withstand the blast load. In contrast, the higher-strength polymer concrete, SPCB-200-1, prevents this damage, highlighting its enhanced blast resistance. Thicker variants, SCB-250-1 and SCB-500-1, positioned 1 m away, demonstrate no visible damage, indicating good blast resistance. Polymer concrete bunkers, specifically SPCB-200-1, SPCB-250-1, and SPCB-500-1, show no signs of cracking or damage at a 1 m distance from a 1 kg TNT explosion, thus highlighting their ability to endure the blast due to the superior strength of polymer concrete.

To seek a more significant impact, Fig. 6 presents the principal stress distribution of bunkers subjected to a 25 kg TNT explosion at a 1 m distance. The SCB-200-25 parades the greatest stress levels compared to other thicknesses, with element removal of 18.1 m^2. Conversely, the higher-strength polymer concrete, SPCB-200-25, prevents element deletions, highlighting its enhanced blast resistance. Thicker SCB-250-25 and SCB-500-25 variants, positioned 1 m away, sustain noticeable damage (16.8 m^2 and 13.05 m^2, respectively), indicating that the blast load surpasses the structures' capacity. This emphasizes the significantly higher potency of a 25 kg TNT explosion, producing a blast wave with greater pressure, impulse, and strain on the buildings compared to a 1 kg TNT explosion. Polymer concrete bunkers with SPCB-200-25, SPCB-250-25, and SPCB-500-25 exhibit no cracking or damage at a 1 m distance from a 25 kg TNT explosion, emphasizing their capacity to withstand the blast due to the superior strength of polymer concrete, which is considered a safer material compared to normal concrete.

Table 4 provides a quantitative comparison of maximum principal stress values for SCB and SPCB configurations at 1 m standoff distance under 1 kg and 25 kg TNT blasts. It includes percentage reductions in stress, highlighting how SPCB offers up to 63% lower stress under high-intensity blasts, demonstrating its superior blast resistance across all thicknesses.

3.3 Damage Pattern on SPCB

Figure 7 provides a detailed visualization of the tensile damage (DamageT) contour plots observed in SPCB when exposed to a 1 kg TNT blast at a distance of 0.25 m, specifically from a top-view perspective. Notably, among the represented thicknesses (200 mm, 250 mm, 300 mm, and 500 mm), Fig. 7a highlights that the 200 mm thickness displays a more pronounced effect compared to the other variations depicted in Fig. 7b, c, and d.

It can be noticed in Fig. 7 that all bunkers maintain structural integrity without facing any obvious damage or crack due to the relatively lower TNT weight. However, SPCB-200-1 experiences a more substantial impact, while SPCB-500-1, as anticipated, demonstrates the least susceptibility to damage, thus matching expectations based on its greater thickness and potential for enhanced resilience against the blast forces.

Figure 8 depicts the tensile damage (DamageT) observed in SPCB subjected to the explosive force of a 25 kg TNT blast at a 0.25 m distance, presenting a *Z*-axis cross-section perspective. Among the represented thicknesses (200 mm,

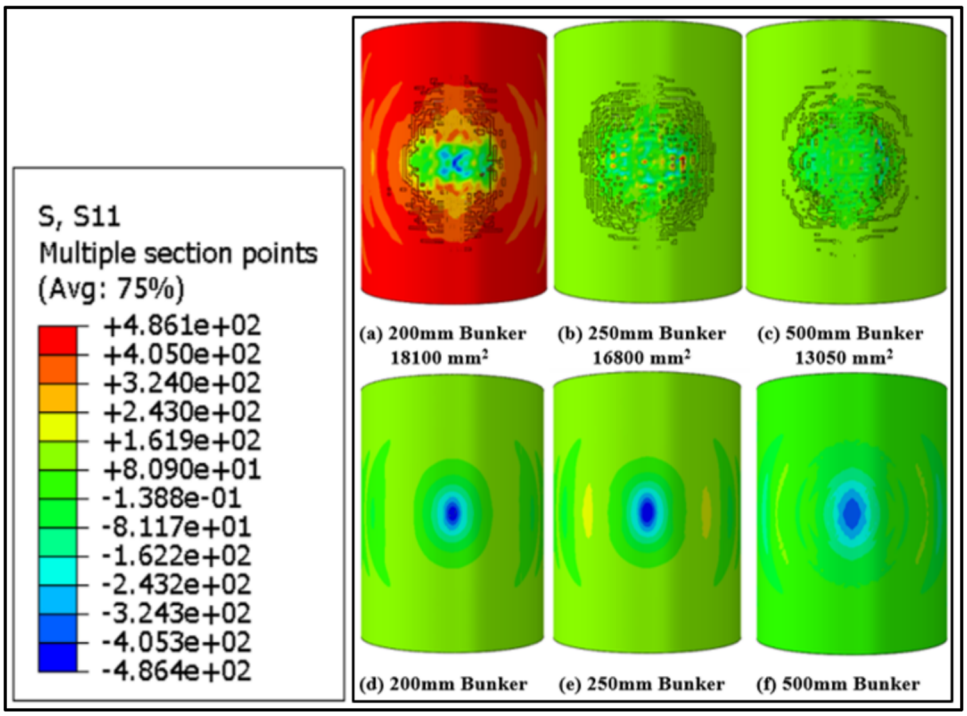

Fig. 6 Principal stress distribution plots of **a**SCB-200-25, **b** SCB-250-25, **c** SCB-500-25 and **d** SPCB-200-25, **e** SPCB-250-25, **f**SPCB-500-25

Table 4 Comparison of maximum principal stress levels for SCB and SPCB bunkers under 1 kg and 25 kg TNT blasts at 1 m standoff distance

Bunker thickness (mm)	TNT (kg)	Standoff distance (m)	Maximum principal stress of SCB (MPa)	Maximum principal stress of SPCB (MPa)	Reduction (%)
200	1	1	52.30	34.07	34.86
250	1	1	30.18	25.11	16.82
500	1	1	18.58	16.54	10.98
200	25	1	120.00	45.00	62.50
250	25	1	108.01	40.05	62.93
500	25	1	90.45	35.08	61.21

250 mm, 300 mm, and 500 mm), Fig. 8a highlights the substantial effect on the bunker with 200 mm thickness, showcasing a significant top surface damage area of 27.99 m^2 and bottom surface damage of 13.24 m^2 compared to Fig. 8b, c, and d. The higher TNT weight leads to observable damage across all bunkers. Specifically, SPCB-250-25 showcases top and bottom surface damage areas with cracking of 21.63 m^2 and 9.08 m^2. SPCB-300-25 exhibits higher top and bottom perforation areas of 13.55 m^2 and 6.96 m^2, respectively, while SPCB-500-25 experiences less damage, with top and bottom damage areas of 3.88 m^2 and 3.78 m^2, due to the increased TNT weight. In general, SPCB-200-25 displays maximum damage with cracks, while SPCB-500-25 exhibits the least effect, matching expectations owing to its greater thickness and capacity for heightened resistance against explosive impact.

When subjected to the impact of a 1 kg TNT blast at a distance of 0.5 m, all the bunkers maintain their structural integrity without experiencing any visible damage or cracking. However, SPCB-200-1 notably demonstrates a more pronounced effect,while SPCB-500-1, due to its greater thickness, showcases minimal to negligible impact, affirming its superior resilience against the relatively lower explosive forces, with the potential for no discernible effect given its substantial thickness.

When exposed to a 25 kg TNT blast at a distance of 0.5 m, the contour plot of SPCB-200-25 in Fig. 9a highlights the noticeable impact on the thinner bunker, displaying a considerable top and bottom surface damage areas of 7.58 m^2 and 3.49 m^2 compared to SPCB-250-25 (Fig. 9b), SPCB-300-25 (Fig. 9c), and SPCB-500-25 (Fig. 9d).

Inspecting the damage site, SPCB-250-25 shows top and bottom perforation areas with cracking of 2.33 m^2 and 2.19 m^2. SPCB-300-25 experiences no damage on the top

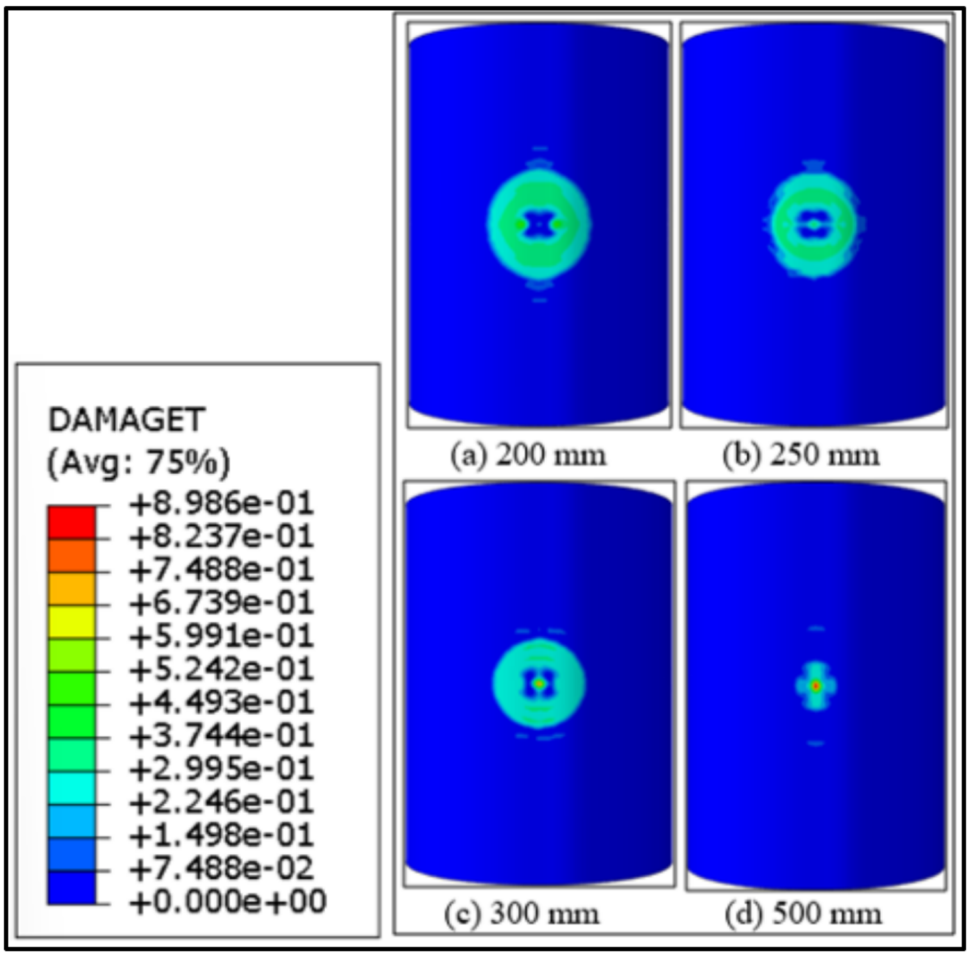

Fig. 7 Tensile damage (DamageT) plots of **a** SPCB-200-1 **b** SPCB-250-1 **c** SPCB-300-1 **d** SPCB-500-1 at 0.25 m blasting distance

surface but displays some material removals with minor cracking, with the bottom surface damage of 3.90 m^2. Similarly, SPCB-500-25 showcases no damage on the top surface but presents minimal material deletion and slight cracking, with 1.43 m^2 of damage on the bottom surface due to the increased TNT weight. To summarize, SPCB-200-25 demonstrates maximum damage with cracks, while SPCB-500-25 exhibits the least effect, aligning with expectations based on its substantial thickness and capability to withstand higher explosive forces.

Under 25 kg TNT blast at a distance of 1 m, SPCB-200-25 in Fig. 10a showcases a noteworthy response,with the top surface demonstrating no damage and no crack, yet registering a bottom surface damage area of 3.25 m^2, or 4.86 m^2 total damage area inclusive of cracks. SPCB-250-25 displays no damage on the top surface but features 3.11 m^2 of the bottom surface exposed reinforcement and 3.65 m^2 of perforation hole. SPCB-300-25 exhibits no damage on the top surface,including no materials deletion, while the bottom surface shows 2.11 m^2 of exposed reinforcement along with 3.54 m^2 of materials deletion.SPCB-500-25 presents no damage on the top surface with no materials deletion, yet encounters 0.1 m^2 of damage in the exposed reinforcement area and 2.22 m^2 of crack area due to the higher TNT weight. Again, SPCB-200-25 sustains maximum damage with cracks,while SPCB-500-25 shows minimal effect, consistent with expectations stemming from the greater thickness, which enhances its resilience against higher explosive forces.

3.4 Damage Areas Comparison of SCB Versus SPCB

In Fig. 11, SCB-200-1 at a 0.1 m stand-off distance exhibits a 1.14 m^2 perforation area on the top surface. Similarly, SCB-250-1 under the same conditions demonstrates a slightly reduced impact, resulting in a 1.05 m^2 perforation hole. In contrast, SCB-500-1 showcases a significantly minimized effect, with only a 0.9 m^2 damage hole on the top surface. Notably, SPCB bunkers with 200 mm thickness, subjected to identical parameters, experience a smaller 0.28 m^2 perforation hole (not shown). Impressively, the 250 mm and 500 mm thicknesses SPCB bunkers demonstrate more robust resistance, remaining undamaged by these forces.

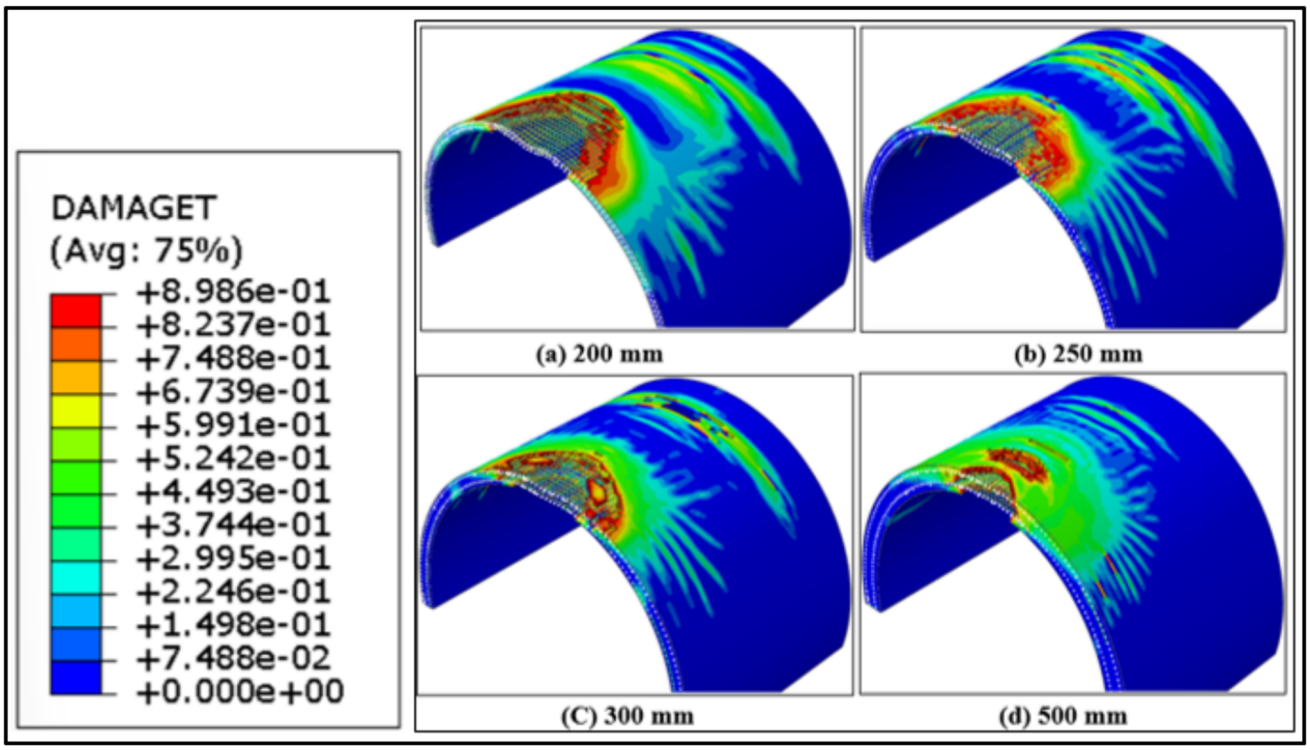

Fig. 8 Tensile damage (DamageT) plots of **a** SPCB-200-25 **b** SPCB-250-25 **c** SPCB-300-25 **d** SPCB-500-25 at 0.25 m blasting distance in *Z*-axis cross-section

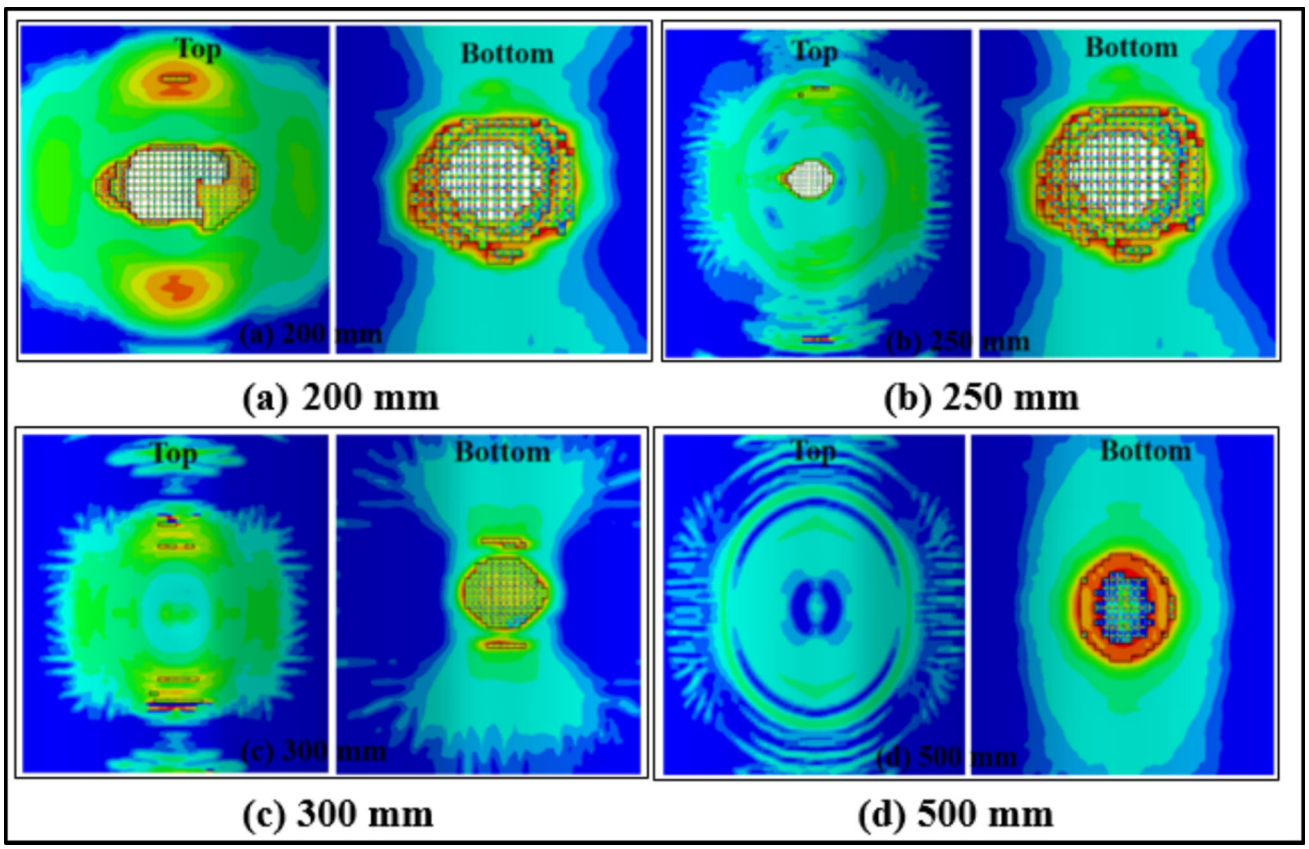

Fig. 9 Tensile damage (DamageT) plots of **a** SPCB-200-25 **b** SPCB-250-25 **c** SPCB-300-25 **d** SPCB-500-25 at 0.5 m blasting distance

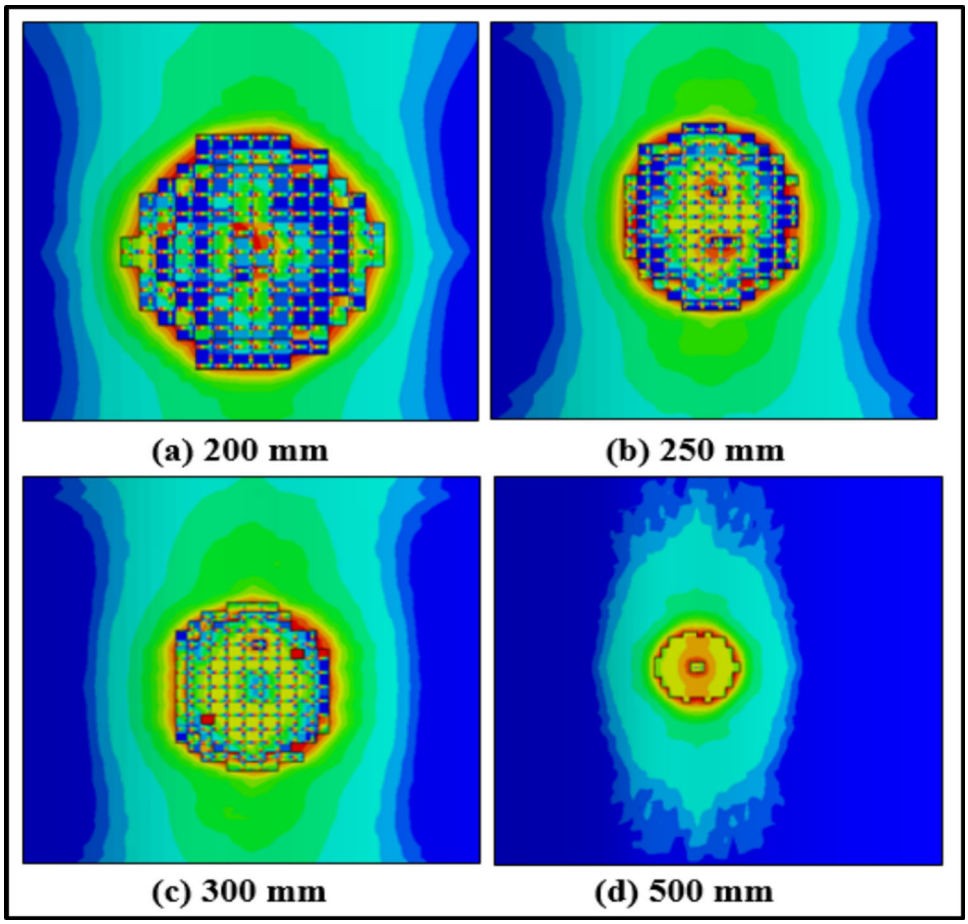

Fig. 10 Tensile damage (DamageT) of **a** SPCB-200-25 **b** SPCB-250-25 **c** SPCB-300-25 **d** SPCB-500-25 at 1 m blasting distance (bottom view)

When subjected to a standard 1 kg TNT charge and placed at a 1 m blasting distance, these bunkers do not incur any discernible damage or hole formation. This absence of damage can be attributed to the combination of lower TNT mass and increased blasting distance employed. Regardless of the bunker type, the reduced TNT mass and a farther blasting distance yield results where none of the cases resulted in any noticeable damage or perforation hole formation. This outcome highlights the significance of the interplay between explosive mass and proximity in determining the structural integrity and resilience of SCB and SPCB bunkers against external forces.

Furthermore, the SCB bunker with a 200 mm thickness, exposed to a substantial 10 kg TNT mass at a 1 m distance, exhibits a notable 11.6 m^2 perforation hole on its top surface. Conversely, SCB-250-10 at the same distance displays a slightly reduced impact, resulting in a 10.9 m^2 perforation hole. SCB-500-10 at the same distance, on the other hand, shows a slightly reduced impact, resulting in a 6.30 m^2 perforation hole. In contrast, SPCB bunkers with 200, 250, and 500 mm thicknesses, under the extreme conditions of a 10 kg TNT mass and a 1 m distance, unveil a remarkable ability to withstand the forces without incurring any damage or hole formation. SCB-200-25 detonated at a 1 m distance exhibits a significant impact resulting in a sizable 18.1 m^2 perforation hole on its top surface. SCB-250-25 at a 1 m distance demonstrates slightly reduced damage, presenting a 16.8 m^2 damage hole on the top surface. Furthermore, SCB-500-25, under identical explosive conditions, displays a reduced impact with a 13.05 m^2 damage hole on the top surface. In stark contrast, all SPCB bunkers subjected to the extreme scenario of a 25 kg TNT mass at a 1 m distance, notably exhibit exceptional resilience by remaining completely undamaged, showcasing no evidence of any damage or hole formation.

As depicted in Fig. 11, both SCB and SPCB bunkers demonstrate good resistance under various blasting scenarios involving 1 kg and 10 kg TNT charges, with significant observable damages at a 1 m blasting distance. Across all cases, the bunkers do not display any damage or hole formation owing to the use of lower TNT masses coupled with a considerable blasting distance. Notably, SCB bunkers exposed to 10 kg TNT and the 2 m blasting distance showcase only minor surface cracks without any discernible damage or hole formation. Conversely, the SPCB bunkers, regardless of

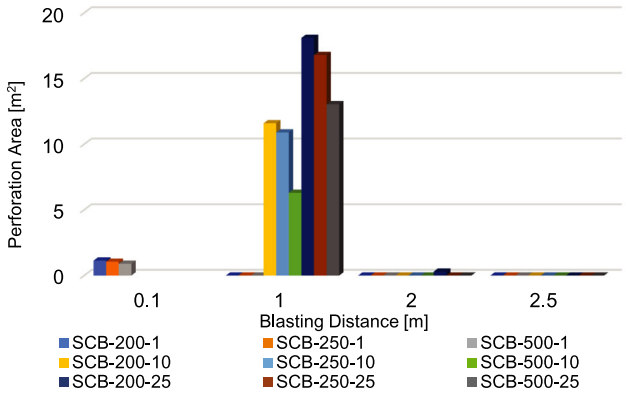

Fig. 11 Perforation area of SCB

the TNT mass and the 2 m blasting distance, consistently exhibit no visible damage or hole formation, highlighting their robustness and ability to withstand these conditions effectively. Across the majority of cases of 25 kg TNT mass detonated at a substantial 2 m distance, both SCB and SPCB bunkers exhibit remarkable resilience, evading any significant damage or hole formation due to the combination of lower TNT mass and the increased distance from the blast zone. However, SCB-200-25 at a 2 m blasting distance displays a minor 0.3 m^2 perforation on its top surface, indicating a slight breach in its integrity. In contrast, the SCB bunkers with 250 mm and 500 mm thicknesses under the same testing conditions show crack lines on their top surfaces without substantial damage or hole formation. Meanwhile, the SPCB bunkers across various thicknesses and the extreme 25 kg TNT charge at the 2 m distance consistently disclose no observable damage or hole formation, highlighting their superior resistance and structural robustness compared to the SCB counterparts in these testing conditions.

At a substantial 2.5 m blast distance, both SCB and SPCB bunkers demonstrate remarkable resilience, showing no visible damage or hole formation. Specifically, in the case of SCB bunkers, under the extreme conditions of 10 and 25 kg TNT charges, those with 200 mm, 250 mm, and 500 mm thicknesses exhibit minor crack lines on their top surfaces, indicative of surface stress, but do not incur substantial damage or hole formation. Conversely, the SPCB bunkers all consistently exhibit no visible signs of damage or hole formation, showcasing their superior structural integrity and capacity to withstand these testing conditions effectively. These findings signify the pivotal role of both TNT mass and the distance from the explosion site in determining bunker resilience, with SPCB configurations demonstrating greater resistance compared to their SCB counterparts.

Here, the comparison elucidates the differences in damage between SCB and SPCB across diverse scenarios. Specifically, deformations in SPCB models consistently prove lower than those in SCB models across all cases. For instance, the 200 mm SCB exhibits a perforation size of 1.402 m^2, contrasting with SPCB's 0.28 m^2. Between the two models, damage varies by 80.03%, with significant differences observed in perforation sizes. The observed variations underscore the effectiveness of polymer concrete with CFRP skin in enhancing specimen stiffness, thereby reducing deformations and resulting in smaller damage areas. Particularly, SPCB models with thin cores (200 mm) demonstrate the most substantial reduction in damage, indicating the success of polymer concrete with CFRP skin in mitigating major damage for thin-core bunkers.

It is worthwhile to realize also that other than a 200 mm thickness, SPCBs show no visible perforation or severe damage. The results confirm that SPCBs exhibit much greater strength and safety in comparison to SCBs, emphasizing their better capacity to resist blasts.

3.5 Regressed Prediction

Upon compiling the data obtained from all models analyzed, a set of regression equations is formulated to describe the principal stress, σ_s, in terms of the input variables of the core thickness (t), TNT mass (m), and standoff distance (d) as:

$$\sigma_s = -159 - 1100d + 44.70m + 2.947t - 26.85dm + 806d^2 - 0.448m^2 - 0.00422t^2 \quad (8)$$

Equation (8) incorporates various factors denoted by t, m, and d, representing specific parameters under examination. The p-values corresponding to d, d^2, m, and dm are all found to be < 0.00, signifying their substantial significance as contributors to the stress equation. Moreover, the m^2 term, although resulting in a p-value of 0.026, is statistically significant, further supporting its influence on the principal stress. Similarly, while the t term yields a p-value of 0.0933, indicating slightly less significance, it is also considered statistically significant within this context.

Furthermore, the mathematical generalization for the von Mises stress (σ_{Mises}) is given by the equation:

$$\sigma_{\text{Mises}} = 179 - 1460d + 78.38m + 1.34t - 37.01dm + 0.669dt - 0.0479mt + 898d^2 - 0.602m^2 - 0.00243t^2 \quad (9)$$

Equation (9) encapsulates multiple variables denoted by t, m, and d, representing distinct parameters considered in the analysis. The p-values corresponding to t, d, d^2, m, mt, and dt are all found to be < 0.00, indicating their substantial significance as contributors to the von Mises stress equation.

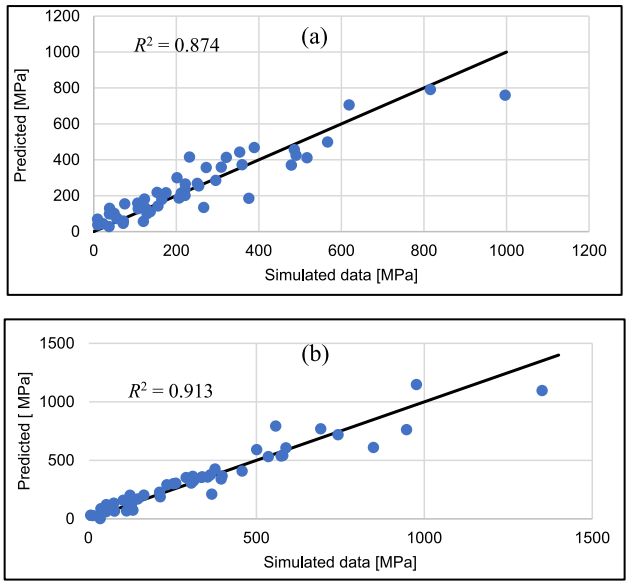

Fig. 12 Comparison of predicted **a** σ_s and **b** σ_{Mises} versus simulation data

Furthermore, although the m^2 term yields a p-value of 0.01 and the t^2 term results in a p-value of 0.109, these factors are deemed statistically significant. Similarly, the mt term, with a p-value of 0.044, also holds statistical significance within this context.

Figure 12a and b present the predictability of Eqs. (8) and (9) in comparison to simulated data, revealing substantial statistical metrics. Equation (8) yields an R^2 value of 87.40%, an adjusted R^2 value of 85.52%, and a predictive R^2 value of 81.49%, depicting robust predictability for σ_s. Similarly, Eq. (9) demonstrates an R^2 value of 91.30%, an adjusted R^2 value of 89.78%, and a predictive R^2 value of 86.29%, signifying strong predictive capabilities for σ_{Mises}. The results show that regression models explain response variable variability using input variables (d, m, and t). Regression equation findings may guide future application design and optimization. It is vital to note that data dependability and accuracy determine forecast accuracy. The regression equations should be validated by experimental observations in future research to provide a more robust and reliable implementation of these models in actual contexts.

4 Conclusion

The blast resistance of semi-circular cross-sectioned cylindrical models, comprising CFRP skins sandwich polymer concrete core bunkers (SPCB) vs. sandwich concrete core bunkers (SCB), with 10 m × 6.5 m × 3.5 m dimensions, has been investigated using ABAQUS/Explicit finite element software incorporating the CONWEP feature. The blasting loads simulating explosions were generated from 1 to 25 kg TNT masses with standoff distances of 0.1–1 m and for sandwich bunkers with core thicknesses of 200–500 mm. The major findings are summarized as follows:

1. The research shows that ABAQUS/Explicit with CONWEP can properly describe bunker behavior under different scenarios for blast-resistant structure design, as verified with existing numerical and experimental results.
2. Generally, increased TNT mass, reduced standoff distance, and thinner core thickness raise deformation and damage severity.
3. SPCBs outperform SCBs, with the 500 mm thick SCB sustaining 34.8% damage from a 25 kg TNT explosion at 1 m. In comparison, SPCB-200-1, SPCB-250-1, and SPCB-500-1 are 80%, 82%, and 99% stronger than SCB-200-1, SCB-250-1, and SCB-500-1, respectively, based on 1 m standoff distance. Other standoff distance cases display a similar advantage of SPCBs.
4. Comparing SCB with the only SPCB model with damage perforation, the variety is 80.03% more. In most cases, SPCB did not reveal any noticeable damage, thus exhibiting SPCB bunkers' superior blast resilience. SPCBs are more durable than SCBs because they seldom perforate.
5. For response estimation and aiding blast-resistant design, general regression equations for principal and von Mises stresses as a function of core thickness, TNT mass, and standoff distance with high predictability have been formulated.

Future research may explore high-performance polymer concrete or geopolymer concrete to improve bunker blast protection [47]. Thicker and more layers of CFRP skins [48–51] by adding steel fiber, polypropylene fiber [52], or textile composite [53–55] to the concrete mix, and using alternative blast-resistant technologies by incorporating sophisticated modeling [56, 57] or machine learning-assisted forecasting [58–61] should also be studied.

Acknowledgements The authors thank Universiti Malaysia Sarawak for VC High Impact Research Grant 2.0 (VC HIRG2.0) under the grant code: UNI/F02/VC-HIRG-2/86080/2023.

Author Contributions All authors contributed to the study conception, design, data analysis, and results discussion. Data collection and the first draft of the manuscript were completed by Mahmudul Hasan. All authors commented, read, and approved the final manuscript.

Funding Open access funding provided by The Ministry of Higher Education Malaysia and Universiti Malaysia Sarawak.

Declarations

Conflict of interests The authors declare that there are no conflicts of interest regarding the publication of this paper.

References

1. Wang, W.; Song, X.; Huo, Q.; Wang, Y.: Experimental and numerical study on local damage effect of ultra-early-strength reinforced concrete slabs (URCS) under contact explosion. Eng. Struct. **294**, 116741 (2023). https://doi.org/10.1016/j.engstruct.2023.116741
2. Buchan, P.A.; Chen, J.F.: Blast resistance of FRP composites and polymer strengthened concrete and masonry structures: a state-of-the-art review. Compos. Part B Eng. **38**, 509–522 (2007). https://doi.org/10.1016/j.compositesb.2006.07.009
3. Choi, J.H.; Choi, S.J.; Kim, J.H.J.; Hong, K.N.: Evaluation of blast resistance and failure behavior of prestressed concrete under blast loading. Constr. Build. Mater. **173**, 550–572 (2018). https://doi.org/10.1016/j.conbuildmat.2018.04.047
4. Shishegaran, A.; Khalili, M.R.; Karami, B.; Rabczuk, T.; Shishegaran, A.: Computational predictions for estimating the maximum deflection of reinforced concrete panels subjected to the blast load. Int. J. Impact Eng **139**, 103527 (2020)
5. Malvar, L.J.; Crawford, J.E.; Morrill, K.B.: Use of composites to resist blast. J. Compos. Constr. **11**, 601–610 (2007). https://doi.org/10.1061/(asce)1090-0268(2007)11:6(601)
6. Yi, N.H.; Kim, J.H.J.; Han, T.S.; Cho, Y.G.; Lee, J.H.: Blast-resistant characteristics of ultra-high strength concrete and reactive powder concrete. Constr. Build. Mater. **28**, 694–707 (2012). https://doi.org/10.1016/j.conbuildmat.2011.09.014
7. Yi, N.H.; Lee, S.W.; Kim, J.W.; Kim, J.H.J.: Impact-resistant capacity and failure behavior of unbonded bi-directional PSC panels. Int. J. Impact Eng **72**, 40–55 (2014). https://doi.org/10.1016/j.ijimpeng.2014.05.005
8. Yi, N.H.; Choi, S.J.; Lee, S.W.; Kim, J.H.J.: Failure behavior of unbonded bi-directional prestressed concrete panels under RABT fire loading. Fire Saf. J. **71**, 123–133 (2015). https://doi.org/10.1016/j.firesaf.2014.11.010
9. Xia, Y.; Wu, C.; Liu, Z.X.; Yuan, Y.: Protective effect of graded density aluminium foam on RC slab under blast loading-an experimental study. Constr. Build. Mater. **111**, 209–222 (2016). https://doi.org/10.1016/j.conbuildmat.2016.02.092
10. Mao, L.; Barnett, S.J.; Tyas, A.; Warren, J.; Schleyer, G.K.; Zaini, S.S.: Response of small scale ultra high performance fibre reinforced concrete slabs to blast loading. Constr. Build. Mater. **93**, 822–830 (2015). https://doi.org/10.1016/j.conbuildmat.2015.05.085
11. Lan, S.; Lok, T.S.; Heng, L.: Composite structural panels subjected to explosive loading. Constr. Build. Mater. **19**, 387–395 (2005). https://doi.org/10.1016/j.conbuildmat.2004.07.021
12. Nurick, G.N.; Langdon, G.S.; Chi, Y.; Jacob, N.: Behaviour of sandwich panels subjected to intense air blast: Part 1—experiments. Compos. Struct. **91**, 433–441 (2009). https://doi.org/10.1016/j.compstruct.2009.04.009
13. Lee, S.W.; Choi, S.J.; Kim, J.H.J.: Analytical study of failure damage to 270,000-kL LNG storage tank under blast loading. Comput. Concr. **17**, 201–214 (2016). https://doi.org/10.12989/cac.2016.17.2.201
14. Fareed, S.; Asad, J.; Khan, A.U.R.: Simulation of reinforced concrete slabs in residential buildings under internal gas blast. Arab. J. Sci. Eng. **50**, 1833–1850 (2024). https://doi.org/10.1007/s13369-024-09100-8
15. Tanrıöver, H.; Şenocak, E.: Nonlinear transient analysis of rectangular composite plates. **49**, 463–468 (2006) https://doi.org/10.1007/978-1-4020-5401-3_64
16. Ha, J.H.; Yi, N.H.; Choi, J.K.; Kim, J.H.J.: Experimental study on hybrid CFRP-PU strengthening effect on RC panels under blast loading. Compos. Struct. **93**, 2070–2082 (2011). https://doi.org/10.1016/j.compstruct.2011.02.014
17. Alhamoud, A.; Tajmir Riahi, H.; Ataei, A.: A practical mix design method of ground granulated blast-furnace slag-based one-part geopolymer concrete. Arab. J. Sci. Eng. **49**, 5447–5466 (2024). https://doi.org/10.1007/s13369-023-08419-y
18. Chin, C.-L.; Ma, C.-K.; Awang, A.Z.; Omar, W.; Kueh, A.B.H.: Stress-strain evaluation of steel-strapped high-strength concrete with modified self-regulating end clips. Struct. Concr. **19**, 1036–1048 (2018). https://doi.org/10.1002/suco.201700134
19. Gargano, A.; Mouritz, A.P.: Comparative study of the explosive blast resistance of metal and composite materials used in defence platforms. Compos. Part C Open Access **10**, 100345 (2023). https://doi.org/10.1016/j.jcomc.2023.100345
20. Almustafa, M.K.; Nehdi, M.L.: Machine learning prediction of structural response for FRP retrofitted RC slabs subjected to blast loading. Eng. Struct. **244**, 112752 (2021). https://doi.org/10.1016/j.engstruct.2021.112752
21. Nayak, A.K.; Shenoi, R.A.; Moy, S.S.J.: Transient response of composite sandwich plates. Compos. Struct. **64**, 249–267 (2004). https://doi.org/10.1016/S0263-8223(03)00135-1
22. Hoo Fatt, M.S.; Pothula, S.G.: Dynamic pulse buckling of composite shells subjected to external blast. Compos. Struct. **92**, 1716–1727 (2010). https://doi.org/10.1016/j.compstruct.2009.12.013
23. Kumar, P.; LeBlanc, J.; Stargel, D.S.; Shukla, A.: Effect of plate curvature on blast response of aluminum panels. Int. J. Impact Eng **46**, 74–85 (2012). https://doi.org/10.1016/j.ijimpeng.2012.02.004
24. Tran, P.; Wu, C.; Saleh, M.; Bortolan Neto, L.; Nguyen-Xuan, H.; Ferreira, A.J.M.: Composite structures subjected to underwater explosive loadings: a comprehensive review. Compos. Struct. **263**, 113684 (2021). https://doi.org/10.1016/j.compstruct.2021.113684
25. Wanchoo, P.; Matos, H.; Rousseau, C.E.; Shukla, A.: Investigations on air and underwater blast mitigation in polymeric composite structures: a review. Compos. Struct. **263**, 113530 (2021). https://doi.org/10.1016/j.compstruct.2020.113530
26. Kumar, P.; Stargel, D.S.; Shukla, A.: Effect of plate curvature on blast response of carbon composite panels. Compos. Struct. **99**, 19–30 (2013). https://doi.org/10.1016/j.compstruct.2012.11.036
27. LeBlanc, J.; Shukla, A.; Rousseau, C.; Bogdanovich, A.: Shock loading of three-dimensional woven composite materials. Compos. Struct. **79**, 344–355 (2007). https://doi.org/10.1016/j.compstruct.2006.01.014
28. Kueh, A.B.H.; Razali, A.W.; Lee, Y.Y.; Hamdan, S.; Yakub, I.; Suhaili, N.: Acoustical and mechanical characteristics of mortars with pineapple leaf fiber and silica aerogel infills–measurement and modeling. Mater. Today Commun. **35**, 105540 (2023). https://doi.org/10.1016/j.mtcomm.2023.105540
29. Jahami, A.; Temsah, Y.; Khatib, J.: The efficiency of using CFRP as a strengthening technique for reinforced concrete beams subjected to blast loading. Int. J. Adv. Struct. Eng. **11**, 411–420 (2019). https://doi.org/10.1007/s40091-019-00242-w
30. Dipika, K.; Tupe, D.H.; Gandhe, G.R.: Dynamic analysis of military bunker subjected to blast. Int. Res. J. Eng. Technol. **07**, 808–814 (2020)

31. Yusuf Shaikh, A.; Shaikh, S.: Review paper on dynamic analysis of military bunkers subjected to air blast. IJASRET Def. J. **6**, 105–110 (2021). https://doi.org/10.51397/OAIJSE06.2021.0018
32. Ghamry Metwally, K.; Zaghw, A.I.; Metwally, K.G.; Emarah, A.M.: Nonlinear dynamic finite element analysis of hardened aircraft shelter subjected to blast load. New York Sci. J. **10**, 59–67 (2017). https://doi.org/10.7537/marsnys101017.08.Keywords
33. Al-Fasih, M.Y.; Kueh, A.B.H.; W. Ibrahim, M.H.: Failure behavior of sandwich honeycomb composite beam containing crack at the skin. PLoS ONE **15**, e0227895 (2020). https://doi.org/10.1371/journal.pone.0227895
34. Abo Sabah, S.H.; Kueh, A.B.H.; Al-Fasih, M.Y.: Bio-inspired vs. conventional sandwich beams: a low-velocity repeated impact behavior exploration. Constr. Build. Mater. **169**, 193–204 (2018). https://doi.org/10.1016/j.conbuildmat.2018.02.201
35. Abo Sabah, S.H.; Kueh, A.B.H.; Bunnori, N.M.: Failure mode maps of bio-inspired sandwich beams under repeated low-velocity impact. Compos. Sci. Technol. **182**, 107785 (2019). https://doi.org/10.1016/j.compscitech.2019.107785
36. Abo Sabah, S.H.; Kueh, A.B.H.; Al-Fasih, M.Y.: Comparative low-velocity impact behavior of bio-inspired and conventional sandwich composite beams. Compos. Sci. Technol. **149**, 64–74 (2017). https://doi.org/10.1016/j.compscitech.2017.06.014
37. Shakil, U.A.; Hassan, S.B.A.: Behavior and properties of tin slag polyester polymer concrete confined with FRP composites under compression. J. Mech. Behav. Mater. **29**, 44–56 (2020). https://doi.org/10.1515/jmbm-2020-0005
38. Yin, H.; Teo, W.; Shirai, K.: Experimental investigation on the behaviour of reinforced concrete slabs strengthened with ultra-high performance concrete. Constr. Build. Mater. **155**, 463–474 (2017). https://doi.org/10.1016/j.conbuildmat.2017.08.077
39. Foglar, M.; Kovar, M.: Conclusions from experimental testing of blast resistance of FRC and RC bridge decks. Int. J. Impact Eng **59**, 18–28 (2013). https://doi.org/10.1016/j.ijimpeng.2013.03.008
40. Tao, Y.; Chen, J.F.; Asce, M.: Concrete damage plasticity model for modeling FRP-to-concrete bond behaviour (2006) https://doi.org/10.1061/(ASCE)CC.1943-5614.0000482
41. O'Higgins, R.M.; McCarthy, M.A.; McCarthy, C.T.: Comparison of open hole tension characteristics of high strength glass and carbon fibre-reinforced composite materials. Compos. Sci. Technol. **68**, 2770–2778 (2008). https://doi.org/10.1016/j.compscitech.2008.06.003
42. Qaddura, M.: Aci318-02-Building-Code-for-Structural-Concrete. Khaled **7**, 65–70 (2020)
43. Kueh, A.B.H.; Wang, X.H.; Chen, Y.; Gui, S.J.: Contesting crack modes modeling of reinforced concrete structure threatened by the progressive rust expansion in rebars in the presence of external load. Constr. Build. Mater. **263**, 120127 (2020). https://doi.org/10.1016/j.conbuildmat.2020.120127
44. Kueh, A.B.H.: Competing reinforced concrete cover crack modes: plain and stainless reinforcements rust growth and load effects. Mater. Today Commun. **43**, 111599 (2025). https://doi.org/10.1016/j.mtcomm.2025.111599
45. Hasan, M.; Kueh, A.B.H.: Blasting resistance of curved sandwich composite concrete bunkers. Struct. Eng. Mech. **91**, 63–73 (2024). https://doi.org/10.12989/sem.2024.91.1.063
46. Mohammadzadeh, B.; Kang, J.; Im, S.: Blast loaded plates: simplified analytical nonlinear dynamic approach. Structures **28**, 2034–2046 (2020). https://doi.org/10.1016/j.istruc.2020.10.043
47. Marini, L.; Mannan, M.A.; Kueh, A.B.H.; Abdullah, A.A.; Abed, F.; Gunasekaran, K.: An analysis of the environmental effects of three types of concrete: ready-mixed, reactive powder, and geopolymer. Ain Shams Eng. J. **15**, 102926 (2024). https://doi.org/10.1016/j.asej.2024.102926
48. Kam, C.Z.; Kueh, A.B.H.; Low, K.B.; Wang, X.Y.; Shek, P.N.: Uniaxial compressive stability of laminated composite plate with localised interfacial degeneration. Mater. Res. Innov. **18**, 109–116 (2014). https://doi.org/10.1179/1432891714Z.000000000940
49. Soufeiani, L.; Ghadyani, G.; Kueh, A.B.H.; Nguyen, K.T.Q.: The effect of laminate stacking sequence and fiber orientation on the dynamic response of FRP composite slabs. J. Build. Eng. **13**, 41–52 (2017). https://doi.org/10.1016/j.jobe.2017.07.004
50. Kam, C.Z.; Kueh, A.B.H.; Shek, P.N.; Tan, C.S.; Md Tahir, M.: Flexural performance of laminated composite plates with diagonally perturbed localized delamination. Adv. Sci. Lett. **14**, 455–457 (2012). https://doi.org/10.1166/asl.2012.4042
51. Kam, C.Z.; Kueh, A.B.H.: Bending response of cross-ply laminated composite plates with diagonally perturbed localized interfacial degeneration. Sci. World J. **2013**, 350890 (2013). https://doi.org/10.1155/2013/350890
52. Nikmatin, S.; Syafiuddin, A.; Kueh, A.B.H.; Maddu, A.: Physical, thermal, and mechanical properties of polypropylene composites filled with rattan nanoparticles. J. Appl. Res. Technol. **15**, 386–395 (2017). https://doi.org/10.1016/j.jart.2017.03.008
53. Kueh, A.B.H.: Fitting-free hyperelastic strain energy formulation for triaxial weave fabric composites. Mech. Mater. **47**, 11–23 (2012). https://doi.org/10.1016/j.mechmat.2012.01.001
54. Kueh, A.B.H.: Buckling of sandwich columns reinforced by triaxial weave fabric composite skin-sheets. Int. J. Mech. Sci. **66**, 45–54 (2013). https://doi.org/10.1016/j.ijmecsci.2012.10.007
55. Rasin, N.; Kueh, A.B.H.; Mahat, M.N.H.; Yassin, A.Y.M.: Stability of triaxially woven fabric composites employing geometrically nonlinear plate model with volume segmentation ABD constitution. J. Compos. Mater. **50**, 2719–2735 (2016). https://doi.org/10.1177/0021998315612538
56. Mokhatar, S.N.; Sonoda, Y.; Kueh, A.B.H.; Jaini, Z.M.: Quantitative impact response analysis of reinforced concrete beam using the smoothed particle hydrodynamics (SPH) method. Struct. Eng. Mech. **56**, 917–938 (2015). https://doi.org/10.12989/sem.2015.56.6.917
57. Mokhatar, S.N.; Abdullah, R.; Kueh, A.B.H.: Computational impact responses of reinforced concrete slabs. Comput. Concr. **12**, 37–51 (2013). https://doi.org/10.12989/cac.2013.12.1.037
58. Kueh, A.B.H.: Artificial neural network and regressed beam-column connection explicit mathematical moment-rotation expressions. J. Build. Eng. **43**, 103195 (2021). https://doi.org/10.1016/j.jobe.2021.103195
59. Tan, W.L.; Lee, Y.H.; Tan, C.S.; Lee, Y.Y.; Kueh, A.B.H.: Mechanical properties and fracture prediction of concretes containing oil palm shell and expanded clay for full replacement of conventional aggregates. Jurnal Teknol. **84**, 171–181 (2022). https://doi.org/10.11113/jurnalteknologi.v84.17485
60. Tang, Y.X.; Lee, Y.H.; Amran, M.; Fediuk, R.; Vatin, N.; Kueh, A.B.H.; Lee, Y.Y.: Artificial neural network-forecasted compression strength of alkaline-activated slag concretes. Sustainability **14**, 5214 (2022). https://doi.org/10.3390/su14095214
61. Yakub, I.; Kueh, A.B.H.; Andres Pineda De La O, E.; Rahman, M.R.; Barawi, M.H.; Abdullah, M.O.; Amran, M.; Fediuk, R.; Vatin, N.I.: Employing an artificial neural network in correlating a hydrogen-selective catalytic reduction performance with crystallite sizes of a biomass-derived bimetallic catalyst. Catalysts **12**, 779 (2022). https://doi.org/10.3390/catal12070779